

24 Tau leptons decay leptonically to an electron or muon (and associated
 25 neutrinos), but such decays are very difficult to distinguish from prompt
 26 leptons. Therefore in the following, we concentrate on hadronic tau decays,
 27 which represent about 65% of the tau lepton branching ratio. Such a decay
 28 is characterized by a small number of collimated tracks (typically one or
 29 three, coming from charged pions) in the tracking detectors with no track
 30 activity in an isolation region around them. The sizable lifetime $c\tau = 87\mu\text{m}$
 31 [2] generates a noticeable transverse flight path. Decaying tau leptons leave
 32 also well collimated energy deposits in the calorimeter, often associated with
 33 strong electromagnetic (EM) component from π^0 produced in tau decays.
 34 Typically the energy deposit in the isolation region around them is small.

35 Since March 2010 the ATLAS [3] experiment at the LHC has been col-
 36 lecting proton-proton collisions events at a centre-of-mass energy of $\sqrt{s} =$
 37 7 TeV. The collected data are used to study the performance of the recon-
 38 struction and identification of hadronic tau decays, as well as the trigger
 39 selection for hadronically decaying tau leptons.

40 The tau trigger is described in Section 2, while the offline tau reconstruc-
 41 tion and identification are presented in Sections 3 and 4. The first observed
 42 processes with hadronically decaying tau leptons with the ATLAS detector
 43 are reported in Section 5.

44 2. Tau trigger

45 In order to ensure the efficient selection of interesting events at data
 46 taking, the trigger system [4] of the ATLAS experiment consists of three
 47 steps: a fast hardware-based Level 1 trigger (L1), and the software High
 48 Level Trigger (HLT), composed of the Level 2 trigger (L2) and the Event
 49 Filter (EF).

50 The L1 tau trigger finds regions of interest (RoI) in the detector. It
 51 uses 0.1×0.1 ($\Delta\eta \times \Delta\phi$) calorimeter towers (sums of several cells) to de-
 52 termine the local maximum above E_T threshold in a 0.2×0.2 region. The
 53 outer cells from the broader 0.4×0.4 region are optionally used to define
 54 an isolation region. The HLT uses RoIs defined by L1 trigger for partial
 55 detector readout. At L2 tracking information is combined with jets made
 56 out of calorimeter cells and the tau identification variables are built. The
 57 algorithm run at EF level is similar to the offline reconstruction procedure
 58 (described in sections 3 and 4), using calorimeter energy clusters with proper
 59 calibration and noise suppression applied. At HLT the selection is based on
 60 rectangular cuts on track and calorimeter cluster variables.

61 The trigger menu is a complete set of triggers covering the full spectrum
 62 of tau physics. It contains:

- 63 • single tau triggers with increasing energy thresholds and identification

64 tightness, which are used for heavy $H \rightarrow \tau\tau$, $Z' \rightarrow \tau\tau$ and $H^\pm \rightarrow \tau\nu$
 65 identification;

- 66 • di-tau triggers designed for heavy resonances;
- 67 • triggers combining taus with another object (to reduce rates): tau+ e/μ
 68 for $Z \rightarrow \tau\tau$, $t\bar{t}$, $H \rightarrow \tau\tau$, SUSY, tau+ E_T^{miss} for $W \rightarrow \tau\nu$, $H^\pm \rightarrow \tau\nu$,
 69 SUSY and tau+(b)jets for $t\bar{t}$ and SUSY.

70 The single tau trigger efficiency is presented in Fig. 1 showing a good
 71 agreement between data and MC for L1, L2 and EF for a minimum bias
 background sample.

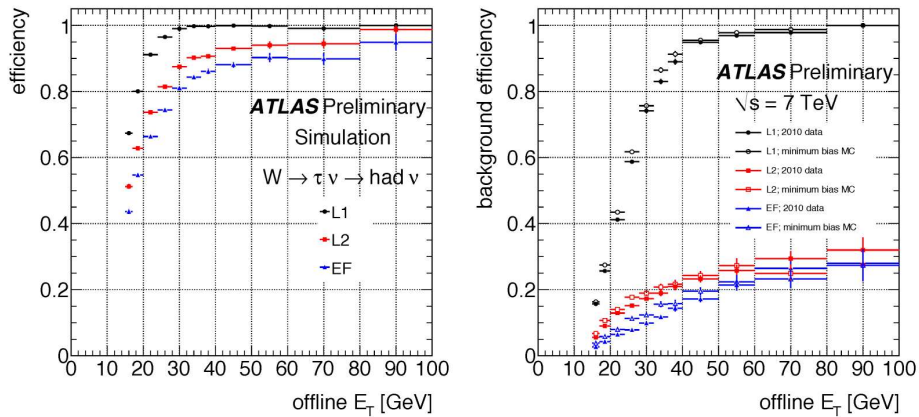


Fig. 1. Fraction of reconstructed tau candidates (no identification applied) passing L1 (5 GeV), L2 (7 GeV) and EF (12 GeV) loose trigger conditions as a function of E_T of the offline candidate. Left: signal efficiency on $W \rightarrow \tau\nu$; right: data-MC comparison on minimum bias background.

72

73 3. Tau reconstruction

74

75 The data collected at centre-of-mass energy of $\sqrt{s} = 7$ TeV recorded
 76 with the ATLAS detector with integrated luminosity of 244 nb^{-1} [5] are
 77 used to study the reconstruction and identification algorithms for hadronic
 tau decays.

78 All events must satisfy the Level 1 trigger condition requiring a tau-
 79 trigger object passing a $p_T = 5$ GeV threshold. In order to select events
 80 with back-to-back jets and therefore enrich the sample with fake tau jets
 81 originating from QCD processes additional selection criteria are applied.
 82 At least one tau candidate with $p_T > 30$ GeV and another one with $p_T >$

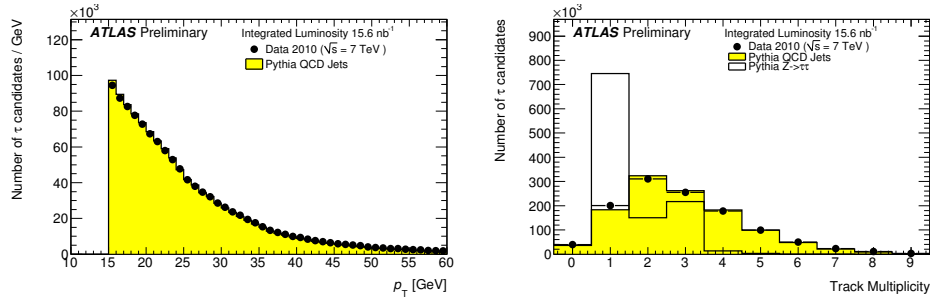


Fig. 2. Transverse momentum distribution (left) and number of associated tracks of τ candidates (right). The number of τ candidates in MC samples are normalised to the number of τ candidates selected in data. The data correspond to an integrated luminosity of 15.6 nb^{-1} .

83 15 GeV are required. They should be separated by at least 2.7 radians in
 84 azimuthal plane. Also the leading tau candidate is excluded to remove any
 85 trigger bias. Data sample selected contains about 2.9 million events with
 86 3.9 million tau candidates.

87 The obtained distributions are compared to the simulated QCD sam-
 88 ples. The transverse momenta of the outgoing partons are restricted to be
 89 between 8 and 280 GeV. These samples are generated with PYTHIA [6] using
 90 the DW tune [7] and passed through a GEANT4 simulation of the ATLAS
 91 detector [8]. When showing distributions for true tau candidates, a $Z \rightarrow \tau\tau$
 92 MC sample with the MC09 tune [9] is used.

93 The reconstruction of hadronically decaying tau leptons starts either
 94 from calorimeter or track seeds [1]. Reconstruction of calorimeter-seeded
 95 tau candidate begins with calorimeter jets reconstructed with the anti- k_t al-
 96 gorithm [10] (using a distance parameter $R = 0.4$) starting from topological
 97 clusters [11]. The candidate is required to have $p_T > 10$ GeV. Track-seeded
 98 candidates are required to have seeding track with $p_T > 6$ GeV and the
 99 tracks with $p_T > 1$ GeV are collected around it in a cone $\Delta R < 0.2$. If jet
 100 seeds are found within $\Delta R < 0.2$, such a candidate is labeled as double-
 101 seeded.

102 Only a small percentage of tau candidates are track-seeded only. In the
 103 studies presented here, candidates with both seeds and candidates with only
 104 a calorimeter-seed with at least one associated track are considered.

105 Figure 2 shows transverse momentum distribution and the number of
 106 associated tracks of the tau candidate (a real tau lepton is expected to have
 107 mostly one or three such tracks). Monte Carlo simulation and data agree
 108 very well.

109

4. Tau identification

110 The tau reconstruction algorithm does not provide large rejection against
 111 QCD jets. Therefore an additional identification (ID) step is necessary. Tau
 112 leptons are difficult to identify and therefore require the full power of ID
 113 variables. A simple cut-based ID as well as more advanced likelihood and
 114 boosted decision tree (BDT) multivariate techniques are used [12]. While
 115 discriminating variables, multivariate techniques and detailed systematic
 116 studies are described in detail in [13], here only the basic identification
 117 based on rectangular cuts is presented. This robust identification method
 118 is used in the analysis of $W \rightarrow \tau\nu$ decays (Sec. 5).

119 Discriminating variables used by the cut-based ID include the EM ra-
 120 dius (E_T -weighted shower width in EM calorimeter), the track radius (p_T -
 121 weighted track width) and the leading track momentum fraction (ratio of
 122 the p_T of the leading track and the total transverse momentum of the tau
 123 candidate). Different cuts are applied for tau candidates with one or with
 124 more tracks. The optimization is done for 30% (tight), 50% (medium) and
 125 60% (loose) signal efficiency. The performance of the tau identification is
 126 evaluated in terms of signal and background efficiencies. Signal efficiency
 127 is defined as $\varepsilon_s = N_{\text{pass,match}}^\tau / N_{\text{match}}^\tau$, where N_{match}^τ is the number of recon-
 128 structed tau candidates that are matched within a cone of $\Delta R < 0.2$ with
 129 a true, hadronically decaying tau lepton with visible transverse momentum
 130 $p_T^{\text{vis}} > 15$ GeV and visible pseudorapidity $|\eta^{\text{vis}}| < 2.5$, reconstructed with
 131 the correct number of associated tracks; while $N_{\text{pass,match}}^\tau$ is the number of
 132 these reconstructed candidates that pass the identification criteria. A sim-
 133 ulated sample of $Z \rightarrow \tau\tau$ decays is used to evaluate the signal efficiency.
 134 The background efficiency is defined as $\varepsilon_b = N_{\text{pass}}^b / N_{\text{total}}^b$, where N_{pass}^b is the
 135 number of the τ candidates that pass the identification criteria, and N_{total}^b
 136 is the number of tau candidates in the dijet selection described earlier.

137 The signal and background efficiencies for the loose, medium and tight
 138 settings of the cut-based ID are shown in Fig. 3 as a function of p_T . The
 139 agreement between data and MC is reasonable. Figure 4 shows background
 140 efficiencies as a function of the number of vertices, which is correlated with
 141 the beam intensity. Increased beam intensities lead to different pile-up
 142 conditions. The stability of the simple cut ID against the presence of pile-
 143 up is satisfactory.

144

5. Observation of real taus in $W \rightarrow \tau\nu$ decays

145 At next-to-next-to-leading order (NNLO), the $W \rightarrow \tau\nu$ signal is pre-
 146 dicted to be produced with a cross section times branching ratio of $\sigma \times BR =$
 147 10.46 nb [14, 15], which is about ten times higher than for $Z \rightarrow \tau\tau$ events.
 148 Events from $W \rightarrow \tau\nu$ production produce predominantly low p_T tau lep-

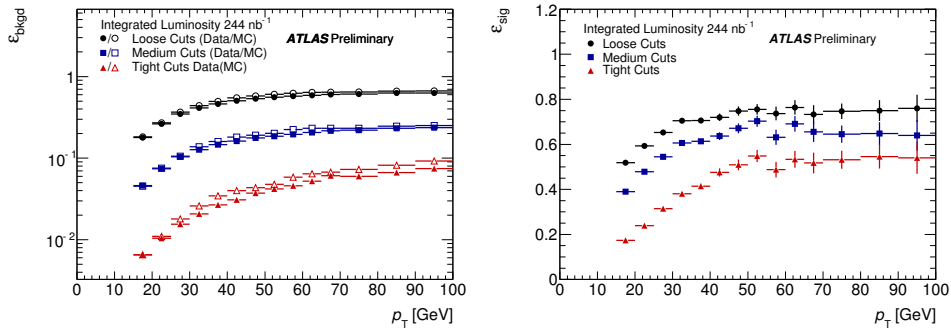


Fig. 3. Background efficiencies obtained for dijet data and MC samples as a function of the reconstructed p_T^τ (left). Signal efficiencies predicted by a $Z \rightarrow \tau\tau$ MC sample as a function of the reconstructed visible p_T^τ (right).

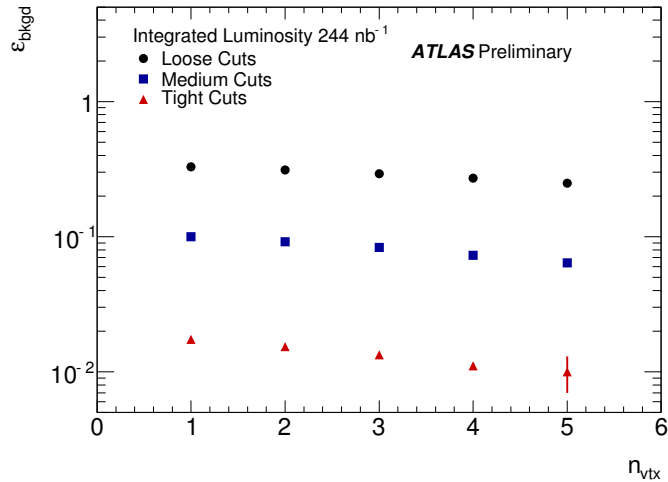


Fig. 4. Background efficiencies as a function of number of vertices n_{vtx} .

149 tons with typical visible transverse momenta between 10 and 40 GeV. In
 150 addition, the distribution of the missing transverse energy, associated with
 151 the neutrinos from the W and tau decays, has a maximum around 20 GeV
 152 and a significant tail up to about 80 GeV.

153 The analysis, described in detail in [16], has been performed on data
 154 collected between March and mid-August 2010. Only data taken during
 155 periods with stable beams and with a good data quality for all the tracking
 156 and calorimeter sub-detectors are used. With these basic data quality cri-

157 teria, the total integrated luminosity available for the analysis amounts to
 158 546 nb^{-1} .

159 Beside additional quality criteria the events are further required to have
 160 the typical $W \rightarrow \tau\nu$ signature, i.e., a tau jet accompanied by missing
 161 energy due to the undetected neutrinos. A missing transverse energy of
 162 $E_{\text{T}}^{\text{miss}} > 30 \text{ GeV}$ is required. Tau candidates must be both-seeded (track and
 163 calo-seeded) and identified as tight tau candidates by cut ID. The highest-
 164 p_{T} candidate of these is selected and required to have a visible transverse
 165 momentum between 20 and 60 GeV. The event is rejected if the selected tau
 166 candidate is reconstructed in the pseudorapidity range $1.3 < |\eta| < 1.7$. Elec-
 167 tron and muon vetoes are applied to suppress the electroweak backgrounds
 168 ($W \rightarrow e\nu$, $W \rightarrow \mu\nu$, $W \rightarrow \tau\nu$, $Z \rightarrow ee$, $Z \rightarrow \mu\mu$ and $Z \rightarrow \tau\tau$). Events with
 169 identified loose electrons [17] or combined muons [1] with $p_{\text{T}} > 5 \text{ GeV}$ are
 170 rejected. The cut-based tau identification provides additional suppression
 171 of electrons and muons.

172 Finally, the event selection includes a requirement on the significance of
 173 the missing transverse energy, defined as $S(E_{\text{T}}^{\text{miss}}) = E_{\text{T}}^{\text{miss}} / (0.5 \cdot \sqrt{\sum E_{\text{T}}})$,
 174 on the basis of the expected $E_{\text{T}}^{\text{miss}}$ resolution as a function of $\sum E_{\text{T}}$ reported
 175 in [18]. Events are rejected if $S(E_{\text{T}}^{\text{miss}}) < 6 \text{ GeV}^{1/2}$. This requirement is es-
 176 sential for the rejection of QCD background, for which lower $S(E_{\text{T}}^{\text{miss}})$ values
 177 are expected than for $W \rightarrow \tau\nu$ events. Figure 5 shows the two-dimensional
 178 distribution of $E_{\text{T}}^{\text{miss}}$ and $\sqrt{\sum E_{\text{T}}}$ for simulated signal, QCD background and
 179 data, together with the $S(E_{\text{T}}^{\text{miss}})$ requirement. The discriminating power of
 180 this requirement is clearly visible.

181 The selection described above results in 78 events. From Monte Carlo
 182 simulation, the expected number of signal events that pass the selection is
 183 55.3 ± 1.4 events. The electroweak background from other W and Z decays is
 184 11.8 ± 0.4 events, where the error is the Monte Carlo statistical uncertainty.

185 A data-driven method is used to estimate the QCD background. It
 186 is based on the selection of four independent data samples, three in QCD
 187 background-dominated regions (control regions) and one in a signal-domina-
 188 ted region (signal region). The samples are selected with criteria on $S(E_{\text{T}}^{\text{miss}})$
 189 and on the tau identification, which are assumed to be uncorrelated. The
 190 following four regions are used in this analysis:

- 191 • Region A: events with $S(E_{\text{T}}^{\text{miss}}) > 6$ and tau candidates satisfying the
 192 tight tau ID using cut-based method
- 193 • Region B: events with $S(E_{\text{T}}^{\text{miss}}) < 6$ and tau candidates satisfying the
 194 tight tau ID
- 195 • Region C: events with $S(E_{\text{T}}^{\text{miss}}) > 6$ and tau candidates satisfying the
 196 loose tau ID but failing the tight ID

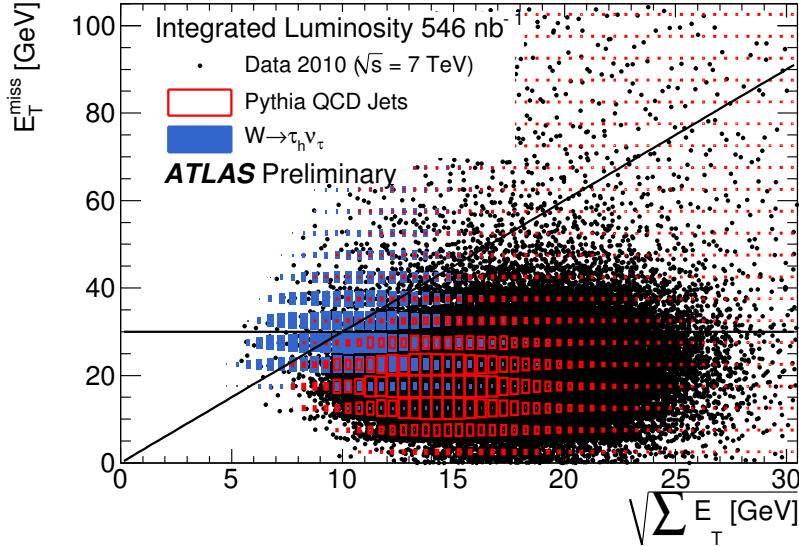


Fig. 5. Distribution of events in the E_T^{miss} vs. $\sqrt{\sum E_T}$ plane after the trigger requirement for data, simulated signal events and QCD background. The applied E_T^{miss} and E_T^{miss} significance cuts are indicated as solid lines.

- 197 • Region D: events with $S(E_T^{\text{miss}}) < 6$ and tau candidates satisfying the
198 loose tau ID but failing the tight ID.

199 This background prediction is based on two assumptions, namely that the
200 shape of the $S(E_T^{\text{miss}})$ distribution for QCD background is the same in the
201 combined regions AB and CD and that the signal and electroweak back-
202 ground contribution in the three control regions is negligible. The es-
203 timate for QCD background in the signal region A is then obtained by:
204 $N_{QCD}^A = N^B N^C / N^D$ where N^i represents the number of observed events
205 in region i .

206 The estimated QCD background is corrected for electroweak backgrounds
207 in the signal and control regions as well as for the non-negligible signal con-
208 tribution in the control regions. To confirm the signal observation, the dis-
209 tributions of the tau track multiplicity, $\Delta\phi(\tau, E_T^{\text{miss}})$, the electric charge of
210 the tau candidates, E_T^{miss} and m_T are compared (see Fig. 6). Here, the data
211 distribution corresponds to the signal region A and the QCD background to
212 the control region C after subtraction of the EW and signal contributions
213 based on Monte Carlo simulation. The distributions are consistent with
214 data.

215 Of the selected 78 events, $11.1 \pm 2.3_{(stat.)} \pm 3.2_{(syst.)}$ events are estimated

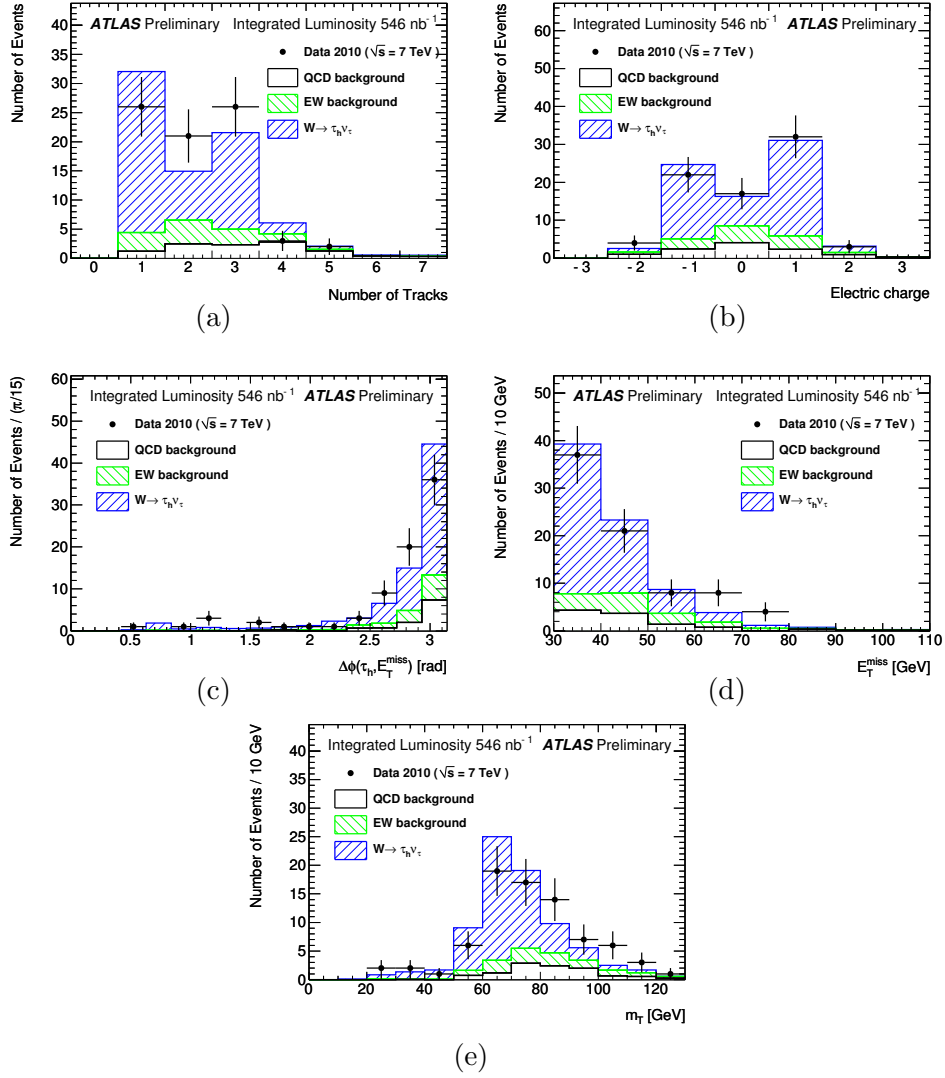


Fig. 6. Distributions of the tau track multiplicity (a), electric charge (b), $\Delta\phi(\tau_n, E_T^{\text{miss}})$ (c), E_T^{miss} (d) and transverse mass m_T (e) for the data in signal region A, the scaled QCD background from control region C, and the contributions from signal and EW background in region A. The QCD background distribution is normalized to the estimated number of QCD background events in region A (N_{QCD}^A).

216 from data to be due to QCD processes. With a remaining background
217 from W and Z decays of $11.8 \pm 0.4_{(stat.)} \pm 3.7_{(syst.)}$ events, estimated from
218 Monte Carlo simulation, this leaves an observed signal of $55.1 \pm 10.5_{(stat.)} \pm$
219 $5.2_{(syst.)}$ events. It is compatible with a Standard Model expectation of
220 $55.3 \pm 1.4_{(stat.)} \pm 16.1_{(syst.)}$ events from $W \rightarrow \tau\nu$ decays. This is the first
221 observation of $W \rightarrow \tau\nu$ decays and of hadronically decaying tau leptons in
222 ATLAS.

223 6. Conclusions

224 Different tau reconstruction and identification algorithms have been de-
225 veloped by the ATLAS collaboration. During the first period of data taking
226 the focus was on robust performance and understanding the discriminating
227 variables rather than optimal performance. The good agreement between
228 data and Monte Carlo in all identification variables and in background rejec-
229 tion rates motivates the use of more sophisticated multivariate techniques
230 (projected likelihood, boosted decision trees) and more identification vari-
231 ables to improve the tau selection performance.

232 The first observation in ATLAS of $W \rightarrow \tau\nu$ decays confirms the detector
233 capability to observe hadronic tau decays. An observation of the $Z \rightarrow$
234 $\tau\tau$ process will be a further confirmation of the ATLAS ability to detect
235 hadronically decaying tau leptons and will be used to further study tau
236 lepton identification at ATLAS.

REFERENCES

- 237 [1] ATLAS Collaboration, Expected performance of the ATLAS experiment: de-
238 tector, trigger and physics, CERN-OPEN-2008-020, 2008.
- 239 [2] K. Nakamura et al. (Particle Data Group), JP G 37 075021, 2010.
- 240 [3] The ATLAS Collaboration, The ATLAS Experiment at the CERN Large
241 Hadron Collider, JINST 3 (2008) S08003.
- 242 [4] ATLAS Collaboration, Performance of the ATLAS tau trigger in p-p collisions
243 at $\sqrt{s} = 7TeV$, ATLAS-CONF-2010-090, 2010.
- 244 [5] The ATLAS Collaboration, Luminosity Determination Using the ATLAS De-
245 tector, ATLAS-CONF-2010-060 (2010).
- 246 [6] T. Sjostrand, S. Mrenna, and P. Z. Skands, PYTHIA 6.4 Physics and Manual,
247 JHEP 05 (2006) 026.
- 248 [7] R. Field, Min-Bias and Underlying Event at the Tevatron and the LHC, talk
249 at the Fermilab MC Tuning Workshop (Oct 2002).
- 250 http://www-cdf.fnal.gov/physics/conferences/cdf8547_RDF_TeV4LHC.pdf

- 251 [8] The ATLAS Collaboration, The ATLAS Simulation Infrastructure,
252 Eur.Phys.J.C70:823-874,2010.
- 253 [9] The ATLAS Collaboration, ATLAS Monte Carlo tunes for MC09, ATL-PHYS-
254 PUB-2010-002 (2010).
- 255 [10] M. Cacciari and G. P. Salam. Phys. Lett. B 641 (2006) 57; M. Cacciari, G. P.
256 Salam and G. Soyez, <http://fastjet.fr/>.
- 257 [11] The ATLAS Collaboration, Calorimeter clustering algorithms: Description
258 and performance, ATL-LARG-PUB-2008-002 (2008).
- 259 [12] ATLAS Collaboration, Tau reconstruction and identification performance in
260 ATLAS, ATLAS-CONF-2010-086, 2010.
- 261 [13] See talk of A. Zemla, Performance of tau lepton identification in ATLAS 7 TeV
262 data, in these proceedings.
- 263 [14] W. Lampl et al., Calorimeter clustering algorithms: description and perfor-
264 mance, ATL-LARG-PUB-2008-002, 2008.
- 265 [15] M. Cacciari, G. P. Salam and G. Soyez, The anti-kt jet clustering algorithm,
266 JHEP 04 063, 2008.
- 267 [16] ATLAS Collaboration, Observation $W \rightarrow \tau\nu$ Decays with the ATLAS Exper-
268 iment, ATLAS-CONF-2010-097, 2010.
- 269 [17] ATLAS Collaboration, Electron and photon reconstruction and identification
270 in ATLAS: expected performance at high energy and results at $\sqrt{s} = 900$ GeV,
271 ATLAS-CONF-2010-005.
- 272 [18] ATLAS Collaboration, Performance of the Missing Transverse Energy Re-
273 construction and Calibration in Proton-Proton Colisions at a Center-of-Mass
274 Energy of 7 TeV with The ATLAS Detector, ATL-CONF-2010-057.